A BIOPOLYMERIC CHITOSAN-ALGINATE NANOCARRIER ENHANCES FLUCONAZOLE EFFICACY IN ANTIFUNGAL THERAPY AGAINST RESISTANT *CANDIDA*

Henry Kolge[1], Gokul Patil[1], Shivaprakash M. Rudramurthy[2], Arunloke Chakrabarti[2], Sachin Jadhav[1] and Vandana Ghormade[1*]

[1]Nanobioscience Group, Agharkar Research Institute, GG Agarkar Road, Pune 411004, India.

[2]Department of Medical Microbiology, Postgraduate Institute of Medical Education and Research, Chandigarh 160012, India.

ABSTRACT

Fluconazole, an antifungal drug faces problems of resistance due to its extensive use. Recently, biopolymeric drug nanocarriers were reported for their favorable characteristics like improved drug efficacy, biocompatibility, reduced toxicity and sustained release. Here, chitosan-alginate nanoparticles (C-Alg-NPs, 115 nm, + 37 mV charge) were fabricated by ionic gelation and loaded with fluconazole (C-Alg-Fluc NPs) having 8 weight % drug loading. The nanoformulation displayed pH-responsive (80 %) release at pH 4 in 5 d while it was low (~ 30 %) at physiological pH 7. The nanoformulation caused 1.8-fold reduced efflux activity (an antifungal resistance mechanism) in *Candida albicans* and resistant *Candida auris* as compared to the bare drug. C-Alg-NPs tagged with Cy5.5 fluorescent dye were localized in fungal cell membrane/cell wall which contributed to reduced efflux activity of fungal pathogen. The nanoformulation displayed a significantly improved 64- and 128-fold *in vitro* antifungal activity (MIC90 2.5 µg/ml) against *C. albicans* and *C. auris*, respectively, as compared to fluconazole. *In-vivo*, C-Alg-Fluc NPs displayed high efficacy against *C. albicans* and *C. auris* infected mice and reduced toxicity as compared to the bare drug. Thus, C-Alg nanocarriers are a promising antifungal treatment and can contribute to reduction of drug resistance.

KEYWORDS: Alginate nanoparticles, chitosan, fluconazole delivery, antifungal nanocarrier, *Candida albicans*, *Candida auris*.

1. INTRODUCTION

Fungal infections are a growing public health problem especially among immunocompromised patients with more than 150 million suffering from systemic fungal infections.[1] Opportunistic fungal species from genera *Candida*, *Aspergillus* and *Cryptococcus* are responsible for > 90 % mortality.[2] Other fungi such as *Penicillum marfenii, Absidia* spp., *Fusarium* spp. affect immunocompromised hosts causing high morbidity and mortality.[3] Recently, a surge in the mucormycosis and aspergillosis cases was reported due to decreased immunity during COVID19 contagion.[4] The alarming situation for these fungal pathogen underline the requirement for effective control. The resistance of these fungi to conventional antifungals confounds the therapeutic strategies.

The current therapeutic options available to combat life-threatening invasive fungal infections are limited. Although the polyene drug amphotericin B is highly effective, it also displays high nephrotoxicity. Echinocandin, a novel antifungal class targeting the glucan cell wall synthesis, faces growing reports of resistance.[5] Fluconazole, a commonly prescribed third generation azole antifungal drug has good tissue distribution, less toxicity, and broad-spectrum activity against *Candida, Cryptococcus* and other fungi.[6-7] Azoles inhibit the cytochrome P450 enzyme lanosterol demethylase (14α-demethylase) leading to accumulation of toxic methylated sterols and interrupting the ergosterol biosynthesis pathway [8]. Inhibition of ergosterol, an essential fungal cell membrane component arrests the cell growth. However, prolonged drug therapy has led to resistance, resulting in clinical failure in immunocompromised HIV patients receiving treatment for *Candida* infection.[9] Drug resistance in *C. albicans* is attributed to its ability to pump azoles out of the cell by plasma membrane located efflux pumps such as ATP-binding cassette transporters (Cdr1p and Cdr2p) and the major facilitator superfamily transporter Mdr1p.[8,10] In the USA, *C. albicans* has a low incidence of fluconazole resistance (0.5–2 %) while *C. tropicalis* (4–9 %)*, C. parapsilosis* (2–6 %) and *C. glabrata* (11–13 %) display higher resistance.[6-7] *Candida auris* is an emerging multidrug resistant yeast that causes major issues regarding patient treatment and surface disinfection in hospitals. *C. auris* strains show >95, 35, and < 4% resistance to fluconazole, amphotericin B and echinocandins, respectively.[11] Lack of newer molecules in the antifungal pipeline make it imperative to explore alternative strategies.[12]

Conventional drugs have constraints such as limited efficacy, poor solubility and toxicity. Nanotechnology strategies for drug delivery improves the bioavailability, solubility, efficacy and reduces the toxicity and provides sustained release.[13-14] Polymeric nanoparticles are extensively studied as drug carriers due to their biocompatibility, biodegradability, functionalization, and sustained release properties.[15] Nanoparticles synthesized from natural polymers are benign, biocompatible and cost-effective as compared to synthetic polymer nanoparticles. Natural polymeric alginate nanoparticles are extensively reported for anti-tuberculosis, -cancer, and -diabetic drug delivery.[16-17] Alginate is a linear copolymer composed of 1-4 linked *α*-L-guluronate (G) and *β*-D-mannuronate (M) monomers. The combination of alginate with other polymers can provide specific mechanical strength, gelation, and cell affinity.[17] Chitosan is a natural, safe, biocompatible, and biodegradable linear cationic polysaccharide composed of D-glucosamine and *N*-acetyl D-glucosamine.[18] Application of chitosan has increased in drug delivery due to its adherence and membrane permeating properties.

Our previous study employing an artificial polymer (polylactide co-glycolide, PLGA) for nanoparticulate drug delivery achieved improved drug efficacy to overcome the pathogen resistance.[22] Artificial polymers like PLGA are expensive and not easily available. Natural polymers are readily available, cost-effective and are widely applied. Therefore, the

current study aims to use a biopolymeric nanoparticulate drug delivery system for antifungal drug delivery. In this study, chitosan-alginate nanoparticles were synthezized by ionotropic pre-gelation method and showed high fluconazole loading. The nanocarrier displayed pH-responsive drug release at pH 4, which is associated with periplasmic space between the fungal cell wall and cell membrane, thereby corroborating our hypothesis. The C-Alg-NPs reduced the efflux activity of *C. albicans* and *C. auris* cells due to the localization of nanoparticles in pathogen cell membrane/cell wall. The nanoformulations showed a significant reduction in antifungal activity against *C. albicans* and *C. auris* as compared to bare fluconazole. C- Alg-NPs were highly effective *in vivo* against *C. albicans* and *C. auris* infected mice and showed high efficacy and reduced toxicity as compared to the bare fluconazole. Alginate nanocarriers reduced the effective drug concentrations required for *C. albicans* and *C. auris* control and can be used for selective drug delivery and reduction in resistance. Thus, biopolymeric nanoformulations display good promise in enhancing drug efficacy, reducing toxicity and overcoming the problem of resistance.

2. MATERIALS AND METHODS

2.1. Synthesis of biopolymeric chitosan-alginate nanoparticles and characterization

Chitosan-alginate nanoparticles were synthesized by ionic pre-gelation method.[23] In pre-gelation step, 0.05% sodium alginate (S.D. fine chemicals, India) was sonicated in distilled water (20 ml) for 30 min, and calcium chloride (5.25 ml, 18 mM, Himedia, India) was added dropwise while stirring. Further, 5.25 ml of chitosan (75 % deacetylated, Sigma Aldrich, USA) solution (0.5 mg/ml in 0.1 M acetic acid, Spectrochem, India) was added with stirring. The chitosan-alginate nanoparticles (C-Alg-NPs) formed were heated at 60 °C for 15 min for hardening, followed by centrifugation at 12000 g for 30 min at 4°C and the pellet was lyophilized.

2.2. Drug Loading of C-Alg-NPs and their characterization

Drug loading was carried out during NPs synthesis by dropwise addition of 1ml fluconazole (2.5 mg in 1 ml of acidified methanol, Sigma Aldrich, USA) after the pre-gelation step, as described in section 2.1, under stirring for 1 h. After addition of 5.25 ml chitosan solution the resultant chitosan-alginate-fluconazole nanoparticles (C-Alg-Fluc-NPs) were heated at 60 °C, 15 min and centrifuged at 12000 g for 30 min at RT.

Drug loading was estimated in supernatant by measuring absorbance at 260 nm in Biotek Synergy HT plate reader. The % drug loading and weight percent loading was calculated according to Chopra et al.[24]

$$\text{Drug Loading} = \frac{\text{Total drug used - Drug in supernatant}}{\text{Total drug used}} \times 100$$

$$\text{Drug Loading (Weight percent)} = \frac{\text{Drug loading}}{\text{Dry weight of nanoformulation}} \times 100$$

Absorbance of 10-50 μg/ml fluconazole was taken at 260 nm to generate the standard graph. Further, C-Alg-Fluc NPs were lyophilized (6h) for calculation of weight percent of drug in the nanoformulation. Bare and fluconazole loaded C-Alg-NPs were characterized for their size and charge by NanoSight Nanotracking Analysis (NTA 2.3, UK), DLS (Beckman Coulter, USA), SEM (Zeiss EVO MA15, Germany), and zeta sizer (Malvern Zetasizer Nano ZSP-90, UK). Drug loading on the nanoparticles was characterized by the presence of characteristic peaks by Fourier Transform Infrared Spectroscopy (Perkin Elmer, USA) and Raman spectroscopy using Witec, Germany.

2.3. *In vitro* drug release

C-Alg-Fluc-NPs were studied for their release profile at pH 4.0 and 7.0. The nanoformulation (1 mg) was dispersed in 1 ml acetate buffer, pH 4 and PBS, pH 7.0 and incubated at 37 °C till 120 h. Absorbance was noted at 260 nm intermittently for 5 d in the supernatant, after centrifugation of nanoformulation at 12000 g for 5 min. The release experiment was performed in triplicates. The cumulative drug release was plotted against the square root of time according to Higuchi's model of drug release. $Q = K_H \times t^{1/2}$ where, K_H is the Higuchi dissolution constant, Q is the cumulative percentage drug release at time.[25]

2.4. *In vitro* antifungal assay against standard strains and clinical isolates

Antifungal assay was performed on *Candida* spp. according to CLSI guidelines (M27A2 and M38A2) with minor modifications. Briefly, yeast cultures were inoculated in 1 % YPG (0.3 % yeast extract, 0.5 % peptone, 1 % glucose) broth, 24 h prior to experiment. Yeast counts were taken with a hemocytometer and 10^4 yeast cells were inoculated per well in 96-well plate. Fluconazole and C-Alg-Fluc-NPs of 1.25- 160 μg/ml, with respect to the drug content. Acidified methanol, C-Alg-NPs, untreated cells and plain media were used as control. Plates were incubated for 12, 24 and 48 h for yeast cultures and the absorbance was measured at 600 nm. Minimum inhibitory concentration (MIC-90) was calculated based on cell viability.

2.5. *In vitro* cytotoxicity of C-Alg-NPs

Toxicity of C-Alg-NPs was assessed with NIH3T3 and HepG2 cells grown in Modified Eagle's Medium (MEM pH 7.4) and Dulbecco's MEM (DMEM pH 7.4) in culture flasks for 24 h. After trypsinization, cell count was taken with hemocytometer and 10^4 cells/well were inoculated in 96-well plate. Fluconazole and C-Alg-Fluc-NPs were added at concentrations of 0.25-32 μg/10 μl to the cells. Acidified methanol, bare nanoparticles, untreated cells and media were taken as control. The plates were incubated for 24 and 48 h, followed by replacement of media and addition of 10 μl/well of 5 mg/ml MTT (3-(4,5-dimethylthiazol-2-yl)-2,5-diphenyltetrazolium bromide Sigma Aldrich, USA). After 4 h, the formazan crystals formed were dissolved in the presence of DMSO. Absorbance was measured at 570 nm and cell viability was calculated.

2.5.1. Hemolytic effect of C-Alg-Fluc-NPs

Fresh sheep blood was procured from local butchery by addition of sodium citrate (1 %) and centrifuged at 1000 g, 5 min at RT. The pelleted RBCs were washed thrice with phosphate buffer saline (PBS, pH 7) and 4 % v/v RBC suspension was prepared in 5 % w/v glucose solution (Himedia, India). Test compounds (C-Alg-Fluc-NPs and fluconazole) were diluted in PBS at concentration of 0.28-37 ug/ml. Triton X (0.1 %) was taken as positive control and PBS as negative control. 750 μL of RBC suspension was added to each concentration at 1:1 ratio and incubated at 37 °C for 2 h. After incubation, samples were centrifuged at 2000 rpm for 10 min and RT Absorbance of supernatant was measured at 540 nm and percentage hemolysis was calculated as following:

$$\% \text{ Hemolysis} = [(A-B)/(C-B)] \times 100$$

Where, A = absorbance of test; B = absorbance of PBS; C = absorbance of 0.1 % Triton X

2.6 Localization of fluorescent C-Alg-NPs by confocal microscopy

C. albicans were exposed to Cy5.5 (Invitrogen, USA) tagged C-Alg-NPs to assess the mode of action. Nanoparticles (1 ml) were incubated with fluorescent Cy5.5 dye (5 μl from 1 mg/ml) and stirred in dark for 1 h. *C. albicans* cells (10^5)

were exposed to fluorescent NPs (10 μg) for 4 h, collected by centrifugation and treated with calcofluor white (5 μl from 1 mg/ml, Sigma Aldrich, USA) for cell wall staining. Cells were mounted on glass slide with PBS and observed under confocal microscope (Leica Microsystems) at Cy5.5: Ex/Em maxima 678/694 nm and Calcofluor white: Ex/Em maxima 380/475 nm.

2.7. Effect of C-Alg-NPs on the Rhodamine 6G efflux

Rhodamine 6G (R6G) efflux was determined according to Saibabu et al.[26] Firstly, *C. albicans* cells were grown in YPG liquid (Yeast 0.3 %, Peptone 0.5 %, Glucose 1 %) media overnight. Cells were transferred to fresh YPG media, and 10^8 cells/ml were exposed to 1 ml of PBS (control), C-Alg-NPs, fluconazole drug (0.5 mg/ml), C-Alg-Fluc-NPs (with 0.5 mg/ml drug) and allowed to grow for 5 h. The drug concentration was 50 % of MIC-90. After 5 h, cells were centrifuged (5000 rpm at 4 °C, 10 min), washed with phosphate-buffered saline (PBS, without glucose), and re-suspended at 10^8 cells/ml in PBS without glucose. Cells were then de-energized in the presence of 2-deoxy-2-Ribose (5 mM, Himedia, India) and 2, 4 Dinitrophenol (5 mM, Himedia, India) in PBS (without glucose) for 1 h. These cells were pelleted at 3500 g at 4 °C, 10 min, washed with PBS (without glucose), and resuspended in 1 ml PBS without glucose. Finally, 10 μM R6G was added to 1 ml cells and incubated for 40 min at 30 °C for equilibration. Further, cells were washed (3500 g at 4 °C for 10 min) and re-suspended in 1 ml of PBS with 1M glucose for initiation of energy dependent efflux. Cells were centrifuged at 10,000 g for 1 min at different time points (0, 10, 20, 30, 45 and 60 min) and supernatant was collected. The absorbance was measured at 527 nm.

2.8. *In vivo* antifungal efficacy and toxicity against *C. albicans* and *C. auris* infections in mice

Nanoformulation efficacy study (ARI/IAEC/2019/02) was designed according to the guidelines and performed by administration of antifungal agent to immunocompromised Swiss albino mice (30-35 g) infected with *C. albicans* or *C. auris* and study for fungal colony counts, toxicity and blood biochemistry parameters was carried out after 48 h.[27] Cyclophosphamide, an immunosuppressive drug, was administered to 7-8 week-old mice at 150 mg/kg body weight, 4 days prior and 100 mg/kg body weight, 1 day prior to the infection. On the day of infection, cell-count of freshly sub-cultured *Candida* cells were taken and suspended at 10^6 /ml in sterile 0.9 % saline warmed to 37 °C. Inoculum (0.1 ml) was injected via the lateral tail vein 2 h prior to the start of drug therapy. Animal groups (n=6, with equal male and female in each group) were injected with fluconazole and C-Alg-Fluc-NPs via tail vein at concentrations of 10, 20 and 40 mg/kg. The concentrations of the treatment were fixed based on previous reports of administration of repeated dosed of 10 mg/kg drug (Wiederhold, Najvar, Bocanegra, Kirkpatrick, & Patterson, 2011). The control groups were bare NPs treated, untreated infected and healthy mice.

After 48 h of drug administration, blood was collected from orbital plexus for blood parameter analyses. Animals were euthanized by primarily CO_2 exposure followed by cervical dislocation and the kidneys of each mouse were immediately resected, one kidney was kept in sterile 0.9 % saline at 4 °C for isolation and quantification of yeast cells and the other was stored in formalin for histology studies. The whole kidney stored in saline was homogenized and 10 μl of the homogenate was spread on YPG plates. Colony count was taken 24 h later. Blood biochemistry study for creatinine, blood urea nitrogen (BUN) levels, and histology study was carried out.

2.9. Statistics

Experimental data: Statistical analysis were performed using one way ANOVA with Bonferroni's Multiple Comparison Test using Graph pad prism 9.0. Significance of the data was also analyzed with the software.

3.0 RESULTS

3.1. Synthesis of bipolymeric chitosan-alginate nanoparticles and characterization

The synthesized C-Alg –NPs were 129 ± 26 nm in size by NTA analysis (Figure 1A i). Particle size by SEM analysis was 115 ± 18 nm (Figure 1A ii), in agreement with the DLS analysis. Ionic interactions between –COOH group of alginate, an anionic polymer and-NH_2 groups of chitosan, a cationic polymer lead to the nanoparticle formation. The slight reduction in size of NPs measured by SEM, as compared to NTA analysis, may be attributed to drying during sample preparation. The zeta potential of C-Alg-NPs were 37.9 ± 3 mV.

3.2. Drug Loading of C-Alg-NPs and their characterization

C-Alg-Fluc-NPs showed 85 % drug loading of fluconazole. The weight percent loading of fluconazole was 8 % in C-Alg-Fluc-NPs (Figure 1 E). C-Alg-Fluc-NPs were 130 ± 11 nm and 120 ± 14 nm in size by NTA and SEM, respectively, and had a zeta potential of $+37.5 \pm 2$ mV (Figure 1B i & ii).

FTIR analyses of C-Alg-Fluc-NPs displayed O-H vibrations and C-H stretch 1136 cm^{-1} for triazole ring breathing in Figure 1C, which confirmed fluconazole loading on nanoparticles.[28-29] Stretching of amide, I band of C=O at 1649 cm^{-1} was indicative of chitosan. The bending vibrations of chitosan, N-H (N-acetylated residues, amide II band), and C-H bending were seen at 1513-1522 cm^{-1} and 1464 cm^{-1}, respectively. The peak at 3120 cm^{-1} and 1077 cm^{-1} in Figure. 1C signifies CH stretch and antisymmetric stretch C-O-C, respectively, confirming the presence of alginate.[30]

Raman spectroscopy of the C-Alg-Fluc-NPs confirmed the presence of a triazole group by ring deformation vibrations (1140 cm^{-1}) representing fluconazole. C=C stretch at 1540 cm^{-1} represents another significant peak for fluconazole (Figure 1D). The characteristic peaks of chitosan corresponding to ring stretching vibrations at 969 cm^{-1}, 1325 cm^{-1}, and mainly to epoxy C-H stretching vibration at 2837 cm^{-1}, were noted.[31] The peaks at 1300 cm^{-1} represent carboxylate stretching vibration characterized by symmetric stretching or C–O single bond stretching vibration of alginate (Figure 1D). Symmetric carboxylate stretching vibration at 1413 cm^{-1} also confirms alginate.[31-32] The characteristic peaks were observed in bare fluconazole and C-Alg-NPs (Figure S1 A and B).

3.3. *In vitro* pH-responsive drug release of fluconazole

A slow sustained release of drug was observed for C-Alg-Fluc-NPs at pH 7.0 and 4.0 till 5 d. C-Alg-Fluc-NPs gave initial burst release (45 %) for 12 h at pH 4, followed by a sustained release of the drug till 120 h. Drug release was between 80 % in 120 h at pH 4, implying a pH-responsive release (Figure 1 F). At pH 7, the nanoformulation showed 26 % drug release in 120 h, indicating low release at physiological pH. When C-Alg-Fluc-NPs were exposed to pH 7, for 2, 4, 6, and 12 h followed by exposure to pH 4 till 72 h the drug release improved to 72, 67, 65, and 64 %, respectively (Supplementary information Figure S2 A).

The drug release at pH 4 followed the Higuchi model with high correlation coefficient of 0.94. These results suggested the controlled release of drug from the nanoparticles. The Higuchi constant (K_H) for C-Alg-NPs was 7.2 implying that the formulation displayed a slow sustained drug release pattern (Supplementary information Figure S2 B).

3.4 *In vitro* antifungal efficacy

The C-Alg-Fluc-NPs were tested for their antifungal efficacy against *C. albicans* and *C. auris* and other fungal strains. The MIC-90 value of fluconazole was 80 μg/ml and 160 μg/ml for *C. albicans* and *C. auris*, respectively.

C-Alg-Fluc-NPs had MIC-90 value of 1.25 μg/ml for both *C. albicans* and *C. auris* (Supplementary Table S1). C-Alg-Fluc-NPs reduced the high MIC of fluconazole by 64- and 128-fold for *C. albicans* and *C. auris*. The nanoformulation also displayed a low MIC-90 value (1.25 μg/ml) for other *Candida* strains like *C. glabrata*, *C tropicalis*, *C. krusei* and *C parapsilopsis* in comparison to the bare drug (Supplementary information Table S1). In addition, the MIC (2.5 μg/ml) for *Cryptococcus neoformans* was remarkably low in comparison to the bare drug (MIC >160 μg/ml).

3.5. Localization of fluorescent C-Alg-NPs

The uptake and localization of Cy5.5 tagged nanoparticles by *C. albicans* cells was visualized by confocal microscopy. Figure 2 A (i-iii) reveals the localization of the NPs on *Candida* cell wall/membrane as seen by the overlap of red fluorescence of Cy5.5 and calcofluor blue fluorescence for the fungal cell wall. *Candida* cells unexposed to NPs showed only blue fluorescent cell walls (Figure 2 B i-iii). The positive zeta potential of C-Alg-Fluc-NPs could play a role in the adherence of NPs to the negatively charged membrane of *Candida* cells and the release of the drug (Figure. 2C schematic).

3.6. Effect of C-Alg-Fluc-NPs on the Rhodamine 6G efflux

Energy dependent dye extrusion was initiated by glucose addition to de-energized *Candida* cells containing R6G. After glucose addition, the control cells in PBS showed dye efflux till 60 min indicating active efflux of the dye. At 60 min, bare fluconazole treated cells showed 27 % decreased efflux. In presence of C-Alg-Fluc-NPs, *C albicans* cells showed 48 % decrease of efflux, in comparison to control cells (Figure 2D i).

Exposure to C-Alg-Fluc-NPs led to 42 % decrease in efflux in *C auris* cells indicating the retention of drug/dye within the cells as compared control cells in PBS. Both the *Candida* strains showed reduced efflux in presence of the nanoformulation (Figure 2D ii).

Figure 2C shows the schematic representation of the localization of the C-Alg-Fluc-NPs in fungal cell wall/membrane and the release of drug to inhibit its efflux by inhibition of ergosterol synthesis.

3.7. *In vitro* cytotoxicity

Murine NIH3T3 and human HepG2 cells did not display any toxicity towards C-Alg-NPs at the tested concentrations (1.25 μg to 160 μg/ ml). These results suggested a good biocompatibility of C-Alg-NPs (Figure 3A).

3.7.1 Hemolytic effect of C-Alg-Fluc-NPs

C-Alg-Fluc-NPs showed < 4.5 % hemolytic activity up to 80 μg/ ml, while it was 6.5 % at 160 μg/ ml. Increasing hemolysis 32.5, 49, 66 % was observed in presence of increasing concentrations of bare fluconazole 20, 40, 80 and 160 μg/ ml, respectively. The C-Alg-Fluc NPs reduced the hemolysis of fluconazole by 12-16-fold that could be attributed to its pH-responsive release at pH 7.0 (Figure 3B).

3.8. *In vivo* antifungal efficacy and toxicity studies in *C. albicans* and *C. auris* infected mice

In vivo antifungal efficacy of C-Alg-Fluc-NPs (10, 20 and 40 mg/kg bwt) treatment against *C. albicans* showed no colony growth of the infectious agent when homogenate of resected kidneys of treated mice were plated on YPG agar media (Figure 4A). However, fluconazole treatment at 10, 20 and 40 mg/kg bwt did not eradicate the fungus (Figure 4A).

In the case of *C. auris* infected mice, there was no detectable fungal growth in the presence of C-Alg-Fluc-NPs treatments at 10-40 mg/kg bwt (Figure 4D). There was 10 % growth at the lowest concentration (10 mg/kg bwt) that could be due to resistance of organism at low drug concentration. Significantly, a single dose of CNPs-Alg-Fluc NPs was highly effective in controlling infection by *C. albicans* at 10 - 40 mg/kg bwt and *C. auris* at 20 - 40 mg/kg bwt *in vivo* in mice. Therefore, these studies clearly illustrate the enhanced efficacy and reduced toxicity of C-Alg-Fluc-NPs.

Blood urea nitrogen (BUN) analyses showed increased values for *C. albicans* infected control (33 mg/dL) and fluconazole (24-32 mg/dL) treatments (Figure 4B). C-Alg-Fluc-NPs treatment at all three concentrations (10, 20 and 40 mg/kg bwt) displayed BUN values (10-14 mg/dL) similar to the healthy control. The same trend was observed for creatinine levels where the nanoformulation treatments were similar to the healthy control group (Figure 4B). In case of fluconazole treatments (2.1-2.7 mg/dL) the creatinine values were similar to the infected control (Figure 4B). BUN and creatinine analyses show that the C-Alg-Fluc-NPs contributed to ~2.3- and ~3.3-fold reduced toxicity compared to bare drug.

In the case *C. auris* the BUN and creatinine values displayed a similar trend to *C. albicans*. The BUN levels in infected control (34 mg/dL) and fluconazole treatments (25-29 mg/dL) were similar (Figure 4E). C-Alg-Fluc-NPs (10, 20 and 40 mg/kg bwt) treatment displayed BUN values (12-15 mg/dL) similar to the healthy control. The creatinine levels for nanoformulation treatment (0.6-0.9 mg/dL) were similar to healthy control (0.7 mg/dL) while the creatinine values for fluconazole treatments (2.2-2.5 mg/dL) were similar to the infected control (Figure 4E). BUN and creatinine analyses show that the C-Alg-Fluc-NPs contributed to ~2- and 3- fold reduced toxicity compared to bare drug.

Histopathology findings from kidneys of C-Alg-Fluc-NPs (10, 20 and 40 mg/kg bwt) treated mice revealed absence of kidney damage in case of both *C. albicans* and *C. auris* infections (Figure 4C & F; vii-ix). The infected control and fluconazole treatments (Figure 4C & F; ii, iv-vi) groups showed prominent glomerular degeneration, enlarged and distorted distal tubules and congestion of blood vessels showing hemorrhages.

In hepatoxicity study of *C. albicans* infected mice, fluconazole treatment groups displayed congestion of blood vessels and hepatic hemorrhage, swelling of hepatocytes, enlarged vacuoles and infiltration of mononuclear cells in hepatic parenchyma (Figure 5A iv-vi).

No such variations were observed in C-Alg-Fluc-NPs treated mice, although minimal hemorrhages were observed at the highest concentration (40 mg/kg bwt) (Figure 5A vii-ix; Supplementary information Table S2). These studies clearly demonstrate the enhanced efficacy and reduced toxicity of C-Alg-Fluc-NPs in mice.
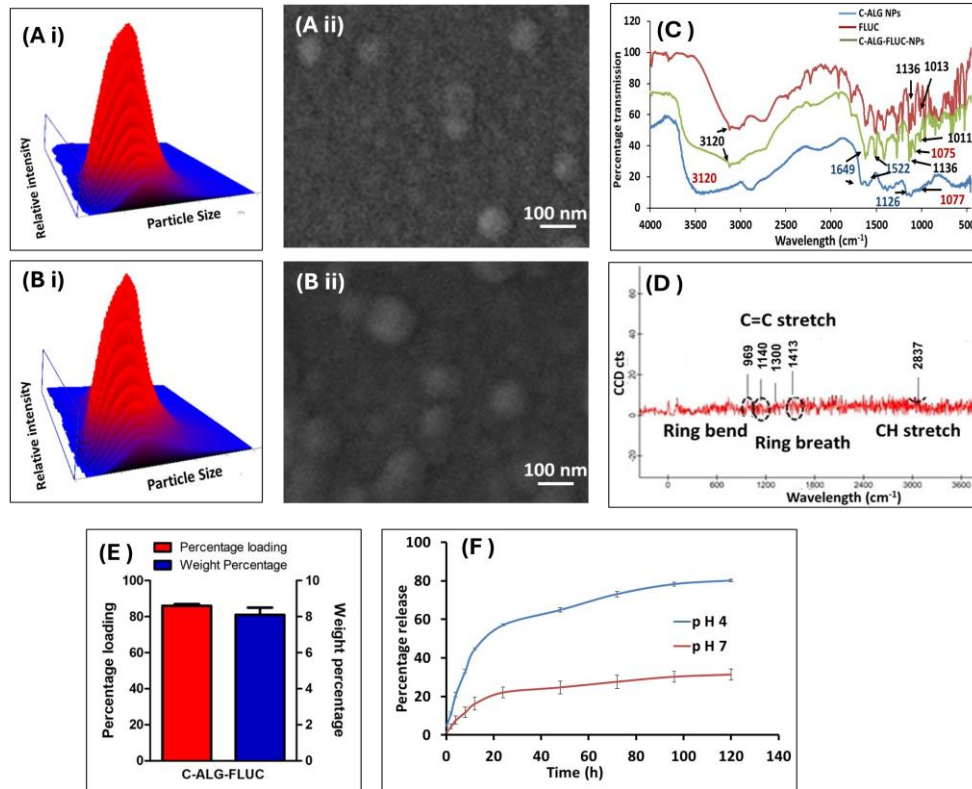
Figure 1: Characterization of nanoparticles A) C-Alg-NPs , B) C-Alg-Fluc-NPs For the panel- i) NTA , ii) SEM; C) FTIR of C-Alg-NPs, Fluconazole, C-Alg-Fluc-NPs D) Raman spectroscopy of C-Alg-Fluc-NPs. E) Drug loading, F) Drug release at pH 4 and 7.
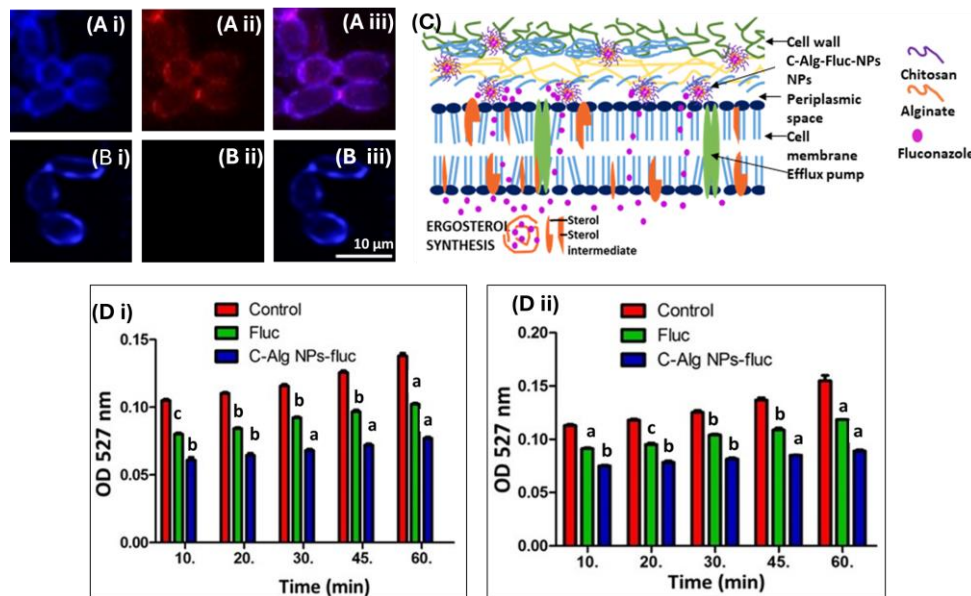

Figure 2: Localization of NPs and R6G efflux assay. Confocal microscopy showing localization of nanoformulation on the surface of *C. albicans* cells in A) C-Alg-NPs treated cells, B) untreated cells; For the panel i) Calcofuor dye for fungal cell wall, blue, ii) Cy5.5 dye for NPs, red, iii) Merged. C) Schematic for localization and release of drug at membrane surface by C-Alg-Fluc-NPs, D) R6G efflux assay in presence of C-Alg-Fluc-NPs treated i) *C. albicans* and ii) *C. auris.* (Significance: a,***, p<0.0001; b,** p<0.001; c,*, p<0.05) in comparison to untreated control at respective time point, using the one way ANOVA: Bonferroni's Multiple Comparison Test).
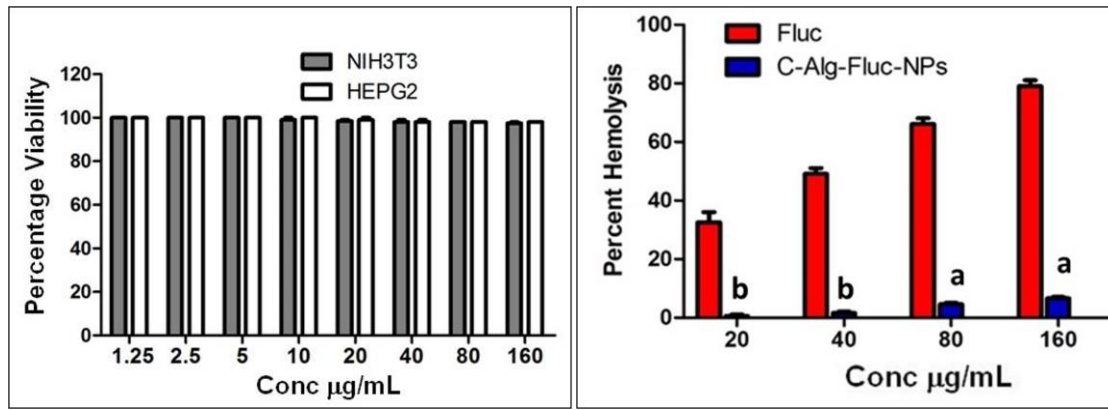
Figure 3: Biocompatibility studies of nanoformulation. Cytotoxicity study of A) C-Alg-Fluc-NPs on NIH-3T3 and Hepg2 cells, B) Hemolytic effect of C-Alg-Fluc-NPs.

(Significance: a,***, p<0.0001; b,** p<0.001; c,*, p<0.05) in comparison to fluconazole at respective concentration, using the one way ANOVA: Bonferroni's Multiple Comparison Test).
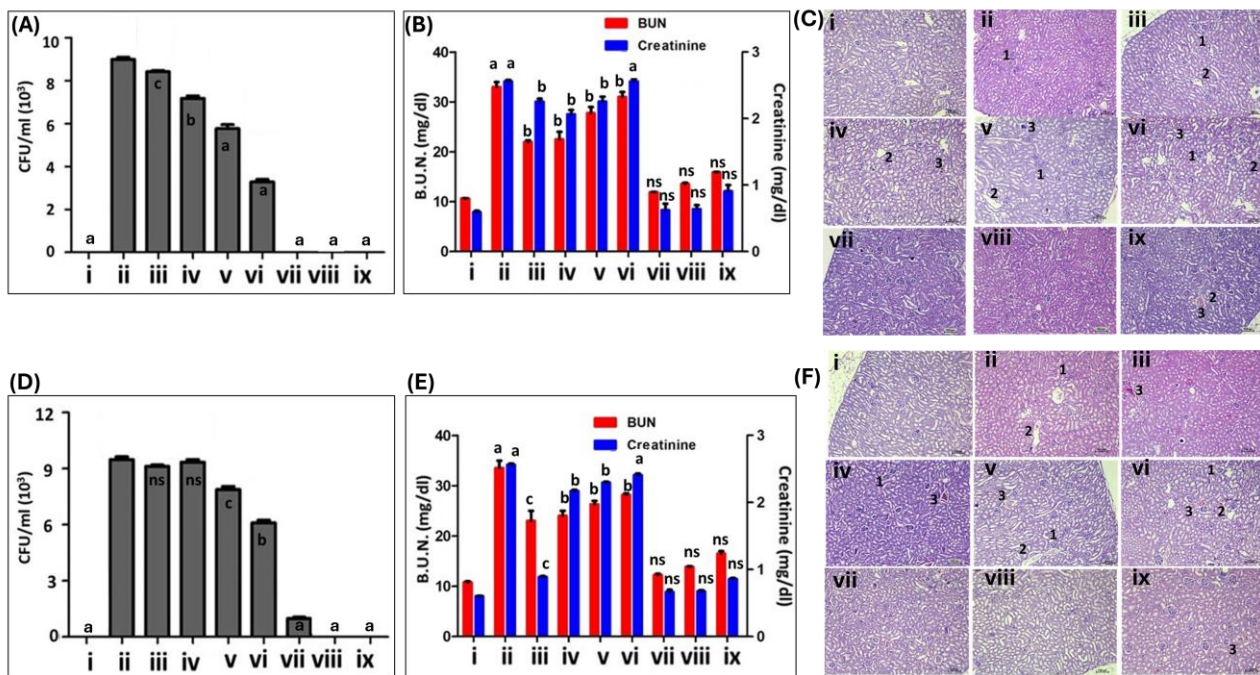

Figure 4: *In-vivo* antifungal and toxicity assay in mice infected with *C. albicans and C. auris*. A and D) Colony count of *C. albicans and C. auris* fungal colonies isolated from kidney, respectively. B and E). BUN/Creatinine levels of *C. albicans and C. auris* infected mice, respectively; C and F) Histological kidney section of *C. albicans and C. auris* infected mice at magnification of 20x, respectively showing 1) glomerular changes like size, atrophy and hypercellularity, 2) enlarged and distorted distal tubules 3) congestion and hemorrhages. Experimental groups for *C. albicans* (A, B, C) and *C. auris* (D, E, F) are i) healthy control, ii) Infected control, iii) C-Alg-NPs, Fluconazole iv) 10 mg/kg, v) 20 mg/kg, vi) 40 mg/kg and C-Alg-Fluc-NPs vii) 10 mg/kg, viii) 20 mg/kg, ix) 40 mg/kg. In B & E) (Significance: a,***, p<0.0001; b,** p<0.001; c,*, p<0.05) in comparison to healthy control, using the one way ANOVA: Bonferroni's Multiple Comparison Test). In C & F) (Significance: a,***, p<0.0001; b,** p<0.001; c,*, p<0.05) in comparison to infected control, using the one way ANOVA: Bonferroni's Multiple Comparison Test).
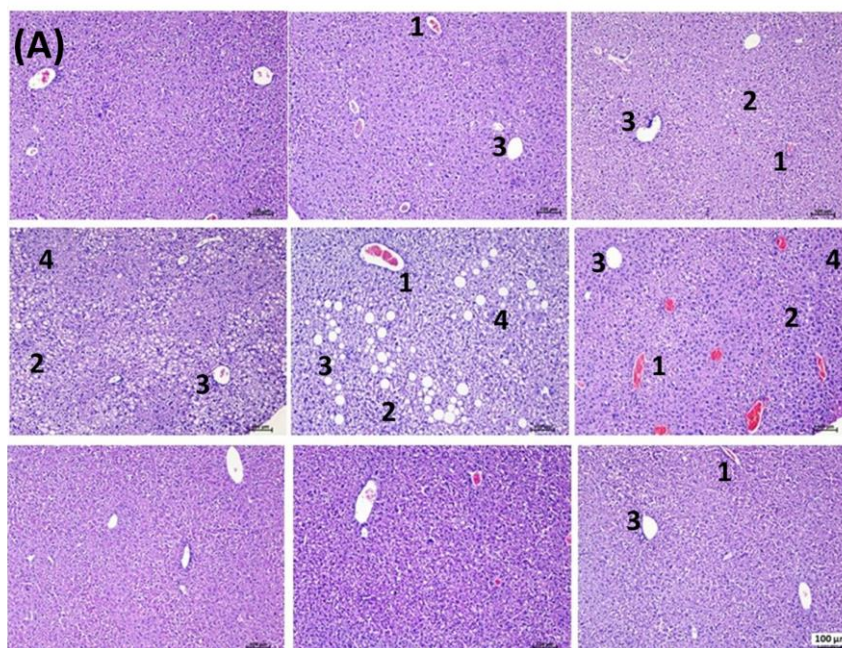
Figure 5: *In-vivo* **hepatotoxicity assay:** Histological study of liver for *C. albicans* at magnification of 20x showing 1) vascular changes-congestion/hemorrhages in hepatic parenchyma 2) cellular changes, swelling of hepatocytes, degenerative and granular cytoplasmic changes, 3) vacuolar cytoplasmic changes; 4) Inflammatory changes in hepatic tissue, mono-nuclear cell infiltration in the hepatic parenchyma. Experimental groups are i) healthy control, ii) Infected control, iii) C-Alg-NPs, Fluconazole iv) 10 mg/kg, v) 20 mg/kg, vi) 40 mg/kg and C-Alg-Fluc-NPs vii) 10 mg/kg, viii) 20 mg/kg, ix) 40 mg/kg.

4. DISCUSSION

The global emergence of multidrug-resistant *Candida* species *like C. auris* is a cause of concern. In view of lack of newer antifungal molecules, nanotechnology can contribute to improved drug delivery, bioavailability, solubility, efficacy and reduce the dosage and toxicity.[33] Polymeric nanoparticles of natural or synthetic origin have potential as drug carriers due to their slow sustained release, low toxicity and biocompatible nature. Previously we reported the use of PLGA, an artificial polymer converted to nanoparticles for fluconazole delivery with improved antifungal efficacy.[22] As part of research strategy to test different polymeric nanoparticles as vectors, we used biopolymers for drug loading. Alginate and chitosan are low-cost naturally available polymers with desirable biocompatibility for the development of drug delivery systems in comparison to synthetic high-cost polymers like poly-lactide coglycolide.[34-35] Furthermore, alginate being anionic complements the cationic backbone of chitosan towards forming a stable nanoformulation.[36] Chitosan polymer with high deacetylation indicates the increased availability of $-NH_2$ groups for ionic interaction. In this study chitosan with 85 % deacetylation was used. Alginate polymer was characterized by FTIR for the ratio of its constituent mannuronate (M) and gluronate (G) groups according to Gómez-Ordóñez & Rupérez.[37] The resultant M/G ratio (1.15) showed a higher proportion of the mannuronate monomer indicating a more flexibility nature of the polymer (Supplementary Information Figure S3). Gómez-Mascaraque et al.[38] have reported that alginate polymers with high M/G ratio displayed increased flexibility as compared to polymers with low M/G ratio. The C-Alg-NPs were synthesized via the pre-gelation method followed by ionic crosslinking of the cationic chitosan and anionic alginate polymers. C-Alg-NPs were 115-129 nm in size with a zeta potential of +37.9 ± 3 mV. C-Alg-Fluc-NPs were 120-130 nm in size with a zeta potential of +37.5 ± 2 mV. The drug-loaded C-Alg-Fluc-NPs were similar in size and

charge to bare nanoparticles. C-Alg-Fluc-NPs showed >80 % drug loading (entrapment) and 8 weight % loading of fluconazole. Previously, Rafiee et al.[39] synthesized chitosan-alginate nanoparticles with 161.8 nm size and +29.3 mV zeta potential. Recently, ionotropically synthesized chitosan alginate nanoparticles were reported with a size of 150 nm and -32 mV zeta potential.[40] Chopra et al., (2014) reported large chitosan nanoparticles (471 nm) with drug loading (63 %). El-Housiny et al.[41] reported 55.49 - 83.04 % fluconazole loading in solid lipid nanoparticles (SLNs) having 85-95 nm size and -20.12 ± 1.88 mV zeta potential.

C-Alg-Fluc-NPs displayed a pH-responsive release at pH 4.0 (80 %) when compared to pH 7.0 (26 %). The pH-responsive nature of nanoformulation was further corroborated by a pH exposure shift from pH 7 to pH 4 that increased drug release to 72 %. Previously, fluconazole loaded chitosan nanoparticles were reported to display less 39 % drug release in 7 h in phosphate buffer.[24] The pH responsive nature of C-Alg-Fluc-NPs was attributed to the presence of chitosan coating on the alginate polymers. Chitosan coated polylactic acid glycolic acid nanoparticles were reported to display a similar response.[22] At pH 4, the chitosan polymers having pKa value (6.3) are protonated and show improved solubility.[42] This leads to loosening of the coating layer and release of fluconazole from the alginate matrix in the C-Alg-Fluc-NPs. Concomitantly, at lower pH, neutralization of carboxylate groups on alginate lowers the negative charges thereby reducing the electrostatic attraction between alginate and drug.[43] Furthermore, Gómez-Mascaraque et al.[38] reported that mannuronate-rich alginates display a weakining of the hydrogel network in low pH. This indicated that administration of nanoformulation at physiological pH did not affect its preferential release at pH 4 in the fungal cell wall/ membrane milieu.

The drug release at pH 4 followed the Higuchi model and showed a diffusion control release from the matrix with a slow sustained drug release pattern. El-Housiny et al.[41] reported that the SLN loaded fluconazole nanoformulation followed the Higuchi pattern of slow sustained drug release upto 24 h.

The periplasmic space between the fungal cell wall and membrane has pH 4-5.[21] This may permit the preferential drug release from C-Alg-Fluc-NPs due to unfolding of chitosan coating, allowing specific antifungal activity (Figure 2D ii). The C-Alg-Fluc-NPs act as vehicle to transport the drug to the cell membrane while the bare drug may not be reaching in sufficient concentration. The mode of action of the nanoformulation is by localization of the C-Alg-Fluc-NPs in fungal cell wall/membrane and the release of drug to inhibit its efflux by inhibition of ergosterol synthesis (Figure 2C). Previously, low molecular weight chitosan polymer was reported for its synergistic activity with fluconazole for inhibition of *Candida*.[44] The cationic nature of chitosan is useful for NPs modification and to improve the drug delivery at the fungal cell wall/membrane interface.[39] Incorporation of cationic chitosan with alginate-based nanoparticles can prolong the contact time with the negatively charged cell membrane to improve absorption.[45] The mode of antifungal action was by penetration and interaction of cationic polymer with the cell membrane. Here we report that the positively charged C-Alg-Fluc-NPs can easily infiltrate the cell wall to adhere with the negatively charged cell membrane for preferential drug release in periplasmic space at low pH. Therefore, the delivery of fluconazole by C-Alg-NPs is due to pH-responsive mode of action.

Remarkably, C-Alg-Fluc-NPs reduced the high MIC of fluconazole by 64- and 128-fold for *C. albicans* and *C. auris*. Recently, fluconazole-loaded SLNs reported MIC-90 of 4 μg/ml against *C. albicans* and *C. glabrata*.[46] Therefore, the preferential localization and pH-responsive release of fluconazole in fungal periplasmic space may be responsible for enhanced *in-vitro* efficacy of nanoformulation. Confocal images show that the C-Alg-NPs were preferentially localized

at the fungal cell wall/membrane interface. Walker et al.[47] entrapped gold nanoparticles in Ambisome, a commercial lipid nanoparticle preparation entrapping amphotericin B, to visualize to its uptake, by transmission electron microscopy (TEM). The uptake of gold liposomes entrapping gold nanoparticles was traced through the fungal cell wall and membrane. Rodrigues et al.[48] employed gold particles labelled with antibodies to trace the movement of ceramide vesicles in fungal membrane, periplasmic space and the fungal cell wall by TEM.

Azole resistance of most clinical isolates of *Candida* are attributed to upregulation of efflux pumps MDR1 and/or CDR1/CDR2 in presence of fluconazole.[49-50] Previously, Maurya et al.[51] demonstrated that inhibition of efflux contributed to retention of fluconazole in the cells. In present study, C-Alg-Fluc-NPs led to 42-48 % decrease in efflux in *C auris* and *C albicans* as compared to fluconazole (27 %) suggesting that the localization of polymeric NPs in *Candida* cell wall/ membrane led to dye retention with the *Candida* cell and that C-Alg-Fluc-NPs were effective in blocking drug efflux.

C-Alg-NPs display good biocompatibility with no toxicity towards murine NIH3T3 and human HepG2 cells. Fluconazole is reported to be non-toxic up to 100 µM (31 µg/ml) in both human hepatoma cell lines.[52] Additionally, C-Alg-Fluc-NPs reduced the hemolysis of fluconazole (12-16 fold) signifying the controlled release of drug from nanoformulation reduces its toxicity and increases its effectivity. Singh et al.[53] reported 55 % hemolysis for fluconazole (64 µg/ ml).

The antifungal effect of C-Alg-Fluc-NPs was assessed in *C. albicans* infected and treated mice by culturing the kidney tissue homogenates. C-Alg-Fluc-NPs (10, 20, and 40 mg/kg bwt) displayed high *in vivo* antifungal efficacy against *C. albicans* infected mice and halted the infectious fungal growth. In comparison, fluconazole treatment showed 20-65 % decrease in fungal growth at mentioned concentration. Similar results were observed for *C. auris* infected mice. Significantly, a single dose of CNPs-Alg-Fluc NPs was highly effective in controlling infection by *C. albicans* at 10-40 mg/kg bwt and *C. auris* at 20-40 mg/kg bwt *in vivo* in mice Therefore, the polymeric nanoformulation displays an improved antifungal efficacy *in vivo* due to controlled drug release as well reduced drug efflux by preferential localization of CNPs-Alg-Fluc NPs to fungal cell wall/membrane.

Although, nanostructured lipids and lipid formulation are reported more often for the delivery of fluconazole their antifungal efficacy is variable. Gupta and Vyas[54] demonstrated that administration of fluconazole-loaded solid lipid nanoparticles and nanostructured lipid carriers *in vivo* in mice reduced the colony count from 10^4 to 10^1 but did not eliminate the infection even after repeated therapeutic treatment. Recently, administration of higher dose of fluconazole (25 mg/kg bwt) *in vivo* in (BALB/C mice) was reported to reduce *C. auris* kidney infection by 37 %, while the commercially available liposomal amphotericin B nanoformulation, Ambisome (3.5-7.5 mg/kg) and bare amphotericin B (0.75 mg/kg) reduced infection by 25-35 %.[55] Previously, a liposomal thymoquinone displaying synergistic activity of thymoquinone with fluconazole (5 mg/kg bwt) was reported for 90 % reduction in kidney fungal *C. albicans* load *in vivo* in BALB/C mice while fluconazole (5-40 mg/kg bwt) led to 50 % reduction.[56]

Recently, fluconazole loaded cubosomal nanoparticles, comprising of lipid bilayer with water channels, were reported for keratomycosis treatment for reduction (<10%) of fungal infection.[57] Polymeric nanocarriers display better stability and controlled release in comparison to lipid based nanocarriers. Recently, a chitosan-coated synthetic polylactide co-glycolide (PLGA) NPs was reported for effective antifungal activity *in vivo* against *C. albicans* and *C. auris*.[22] In

comparison to synthetic polymer NPs, natural polymers are preferably as they can materialize into realistic new generation of drug delivery systems due to their biocompatibility, safety, availability and low-cost.

Furthermore, BUN and creatinine levels in C-Alg-Fluc-NPs treated mice showed ~2.3- and ~3.3-fold reduced toxicity for *C. albicans* and *C. auris* treatments in comparison to bare drug. Histopathology studies showed that C-Alg-Fluc-NPs did not show any damage to the kidney, distal tubules and glomerular structure for both *C. albicans* and *C. auris* infections even at highest concentration. Li et al.[58] reported that fluconazole (30 mg/kg) causes hemorrhages and infiltration of monocytes into the mice kidney. Therefore, these studies clearly illustrate the enhanced efficacy and reduced toxicity of C-Alg-Fluc-NPs.

C. albicans infected mice, fluconazole treatment groups showed hepatotoxicity with prevailing congestion of blood vessels and hemorrhages in hepatic parenchyma, swelling of hepatocytes, enlarged vacuoles and infiltration of mononuclear cells in hepatic parenchyma. Wang et al.[59] showed enlarged hepatocytes, loose cytoplasm, vacuolar degeneration and hemorrhages in fluconazole treated liver sections. Interestingly, no such variations were observed in C-Alg-Fluc-NPs treated mice although minimal hemorrhages were observed at highest concentration (40 mg/kg bwt). These studies clearly demonstrate the enhanced efficacy and reduced toxicity of C-Alg-Fluc-NPs in mice.

5. CONCLUSION

Fungal infections by *C. albicans* and *C. auris* are difficult to control due to their resistance towards azole drugs and require new therapeutic approaches. Recently, biopolymers like chitosan and alginate have been extensively applied as drug nanocarriers due to their favorable characteristics. Here, we synthesized C-Alg-NPs nanoparticles by ionotropic gelation that had a high capacity for fluconazole drug loading and displayed slow sustained drug release. The nanocarrier displayed pH-responsive drug release at acidic pH due to the typical protonation and swelling of chitosan at lower pH. *Candida* cells display a low periplasmic pH that is conducive to preferential drug release by the nanocarrier. This result was corroborated by the localization of fluorescent-tagged nanocarriers on the cell wall/membrane of *Candida* cells. Furthermore, the efflux activity of *C. albicans* and *C auris* was reduced due to C-Alg-Fluc-NPs which prolonged the antifungal activity of fluconazole on pathogen cells to overcome their resistance. Highly effective C-Alg-Fluc-NPs reduced the MIC of fluconazole against *C albicans* (64-fold) and *C. auris* (128-fold) *in vitro*. Administration of C-Alg-Fluc-NPs *in-vivo* to *C. albicans* and *C. auris* infected mice was highly effective in controlling the infection at low nanoformulation concentrations. Moreover, the drug nanocarrier displayed negligible toxicity. Thus, the biopolymeric nanoformulation displays potential for improved antifungal drug delivery and controlling the resistant fungal infections. In future, pharmacodynamics and pharmokinetics studies of these nanoformulation systems are needed to assess their potential for clinical trials.

Ethics approval and Consent to Participate

The *in vivo* study in mice was performed with animal ethics approval (ARI/IAEC/2019/02).

Data availability

The experimental data from this study will be made available from corresponding author upon request.

Declaration of competing interest

The authors declare that they have no known competing financial interests or personal relationships that could have appeared to influence the work reported in this paper.

REFERENCES

1. Rodrigues ML, Nosanchuk JD. Fungal diseases as neglected pathogens: A wake-up call to public health officials. PLoS Negl Trop Dis, 2020; 14: e0007964.

2. Rayens E, Norris KA. Prevalence and Healthcare Burden of Fungal Infections in the United States, 2018. Open forum Infect Dis, 2022; 9: ofab593.

3. Badiee P, Hashemizadeh Z. Opportunistic invasive fungal infections: diagnosis & clinical management. *Indian J Med Res,* 2014; 139: 195.

4. Bhatt K, Agolli A, Patel MH, Garimella R, Devi M, Garcia E, Amin H, Domingue C, Guerra Del Castillo R, Sanchez-Gonzalez M. High mortality co-infections of COVID-19 patients: mucormycosis and other fungal infections. Discoveries (Craiova), 2021; 9: e126.

5. Liu W, Yuan L, Wang S. Recent progress in the discovery of antifungal agents targeting the cell wall. J Med Chem, 2020; 63:12429-12459.

6. Cleveland AA, Farley MM, Harrison LH, Lockhart SR, Magill SS, Chiller TM, Park BJ, Changes in epidemiology of candidemia and antifungal drug resistance in two US locations: results from a population-based active laboratory surveillance, 2008–2010. Clin Infect Dis, 2012; 55: 1352-1361.

7. Berkow EL, Lockhart SR. Fluconazole resistance in *Candida* species: a current perspective. Infect Drug Resist, 2017; 10: 237.

8. Basso LR, Gast CE Jr, Mao Y, Wong B. Fluconazole transport into *Candida albicans* secretory vesicles by the membrane proteins Cdr1p, Cdr2p, and Mdr1p. Eukaryot Cell, 2010; 9: 960–970.

9. Abrantes PM, Fisher R, Bouic PJ, McArthur CP, Fielding BC, Africa CW. HPLC-MS identification and expression of Candida drug-resistance proteins from African HIV-infected patients. AIMS Microbiol, 2021; 7: 320.

10. Prasad R, Kapoor K. Multidrug resistance in yeast *Candida*. Int. Rev. Cytol, 2005; 242: 215–248.

11. Ademe M, Girma F. *Candida auris*: From multidrug resistance to pan-resistant strains. Infect. drug resist, 2020; 13:1287.

12. Pathan EK, Tupe SG, Deshpande MV. Fungal differentiation: A model phenomenon to screen antifungal drugs. In: (Eds. Satyanarayana T, Deshmukh SK, Johri BN), Developments in Fungal Biology and Applied Mycology, Springer Singapore, 2017; 227-246.

13. Kumar R. Nanotechnology based approaches to enhance aqueous solubility and bioavailability of griseofulvin: a literature survey. J Drug Deliv Sci Technol, 2019; 53: 10 1221.

14. Voltan AR, Quindos G, Alarcón KPM, Fusco-Almeida AM, Mendes-Giannini MJS, Chorilli M. Fungal diseases: could nanostructured drug delivery systems be a novel paradigm for therapy? Int. J. Nanomedicine, 2016; 11: 3715.

15. Pontes-Quero GM, Benito-Garzón L, Cano JP, Aguilar MR, Vázquez-Lasa B, Amphiphilic polymeric nanoparticles encapsulating curcumin: antioxidant, anti-inflammatory and biocompatibility studies. Mater. Sci. Eng. C., 2021; 121: 111793.

16. Abdelaziz HM, Gaber M, Abd-Elwakil MM, Mabrouk MT, Elgohary MM, Kamel NM, Kabary DM, Freag MS, Samaha MW, Mortada SM, Elkhodairy KA. Inhalable particulate drug delivery systems for lung cancer therapy: nanoparticles, microparticles, nanocomposites and nanoaggregates, J. Control. Release, 2018; 269: 374–392.

17. Severino P, da Silva CF, Andrade LN, de Lima Oliveira D, Campos J, Souto EB. Alginate nanoparticles for drug delivery and targeting. Curr. Pharm. Des, 2019; 25: 1312-1334.

18. Wang W, Xue C, Mao X. Chitosan: Structural modification, biological activity and application. Int. J. Biol. Macromol, 2020; 164: 4532-4546.

19. Wu D, Zhu L, Li Y, Zhang X, Xu S, G. Yang, T. Delair, Chitosan-based colloidal polyelectrolyte complexes for drug delivery: a review. Carbohydr Polym, 2020; 238: 116126.

20. Zhang H, Wei X, Liu L, Zhang Q, Jiang W. The role of positively charged sites in the interaction between model cell membranes and γ-Fe2O3 NPs. Sci. Total Environ, 2019; 673: 414-423.

21. Plášek J, Babuka D, Gášková D, Jančíková I, Zahumenský J, Hoefer M, nov MA. l method for assessment of local pH in periplasmic space and of cell surface potential in yeast. J Bioenerg Biomembr, 2017; 49: 273-279.

22. Kolge H, Patil G, Jadhav S, Ghormade V. A pH-tuned chitosan-PLGA nanocarrier for fluconazole delivery reduces toxicity and improves efficacy against resistant *Candida*. Int. J. Biol. Macromol*, 2023; 227: 453-461.

23. Sarmento B, Ribeiro AJ, Veiga F, Ferreira DC, Neufeld RJ. Insulin-loaded nanoparticles are prepared by alginate ionotropic pre-gelation followed by chitosan polyelectrolyte complexation. J Nanosci Nanotechnol, 2007; 7: 2833-2841.

24. Chopra AK, Marwaha RK, Kaushik D, Dureja H. Box-Behnken designed fluconazole loaded chitosan nanoparticles for ocular delivery. J.Pharm. Drug Deliv. Res., 2014; 3: 2.

25. Paarakh MP, Jose PA, Setty CM, Christoper GP. Release kinetics–concepts and applications. Int. J. Pharm. Res. Technol, 2018; 8: 12-20.

26. Saibabu V, Fatima Z, Ahmad K, Khan LA, Hameed S. Octyl gallate triggers dysfunctional mitochondria leading to ROS driven membrane damage and metabolic inflexibility along with attenuated virulence in *Candida albicans*. Med. Mycol, 2020; 58: 380-392.

27. Andes D, Marchillo K, Stamstad T, Conklin R. In vivo pharmacokinetics and pharmacodynamics of a new triazole, voriconazole, in a murine candidiasis model. Antimicrob. Agents Chemother, 2003; 47: 3165-3169.

28. Bourichi H, Brik Y, Hubert P, Cherrah Y, Bouklouze A. Solid-state characterization and impurities determination of fluconazol generic products marketed in Morocco. J. Pharm. Anal., 2012; 2: 412-421.

29. Gu XJ, Jiang W. Characterization of polymorphic forms of fluconazole using Fourier transform Raman spectroscopy. J Pharm. Sci., 1995; 84: 1438-1441.

30. Lawrie G, Keen I, Drew B, Chandler-Temple A, Rintoul L, Fredericks P, Grøndahl L. Interactions between alginate and chitosan biopolymers characterized using FTIR and XPS. Biomacromolecules, 2007; 8: 2533-2541.

31. Ren XD, Liu QS, Feng H, Yin XY. The characterization of chitosan nanoparticles by Raman spectroscopy. Appl. Mech. Mater, 2014; 665: 367-370.

32. Schmid T, Messmer A, Yeo BS, Zhang W, Zenobi R. Towards chemical analysis of nanostructures in biofilms II: tip-enhanced Raman spectroscopy of alginates. Anal Bioanal Chem., 2008; 391: 1907-1916.

33. Sousa F, Ferreira D, Reis S, Costa P. Current insights on antifungal therapy: Novel nanotechnology approaches for drug delivery systems and new drugs from natural sources. Pharmaceuticals, 2020; 13: 248.

34. Bakil SNA, Kamal H, Abdullah HZ, Idris MI. Sodium Alginate-Zinc Oxide Nanocomposite Film for Antibacterial Wound Healing Applications. Biointerface Res. Appl. Chem., 2020; 10: 6289–6296.

35. Wang F, Yang S, Yuan J, Gao Q, Huang C. Effective method of chitosan-coated alginate nanoparticles for target drug delivery applications. J Biomater Appl., 2016; 31: 3-12.

36. Niculescu AG, Grumezescu AM. Applications of Chitosan-Alginate-Based Nanoparticles-An Up-to-Date Review. Nanomaterials (Basel), 2022; 12: 186.

37. Gómez-Mascaraque LG, Martínez-Sanz M, Hogan SA, López-Rubio A, Brodkorb A. Nano- and microstructural evolution of alginate beads in simulated gastrointestinal fluids. Impact of M/G ratio, molecular weight and pH. Carbohydr Polym, 2019; 223:115121.

38. Gómez-Ordóñez E, Rupérez P. FTIR-ATR spectroscopy as a tool for polysaccharide identification in edible brown and red seaweeds. Food Hydrocoll, 2011; 25: 1514-1520.

39. Rafiee A, Alimohammadian MH, Gazori T, Riazi-rad F, Fatemi SMR, Parizadeh A, Haririan I, Havaskary M. Comparison of chitosan, alginate and chitosan/alginate nanoparticles with respect to their size, stability, toxicity and transfection. Asian Pac J Trop Dis., 2014; 4: 372-377.

40. Sohail R, Abbas SR. Evaluation of amygdalin-loaded alginate-chitosan nanoparticles as biocompatible drug delivery carriers for anticancerous efficacy. Int J Biol Macromol, 2020; 153: 36-45.

41. El-Housiny S, Shams Eldeen MA, El-Attar YA, Salem H, Attia D, Bendas ER, El-Nabarawi MA. Fluconazole-loaded solid lipid nanoparticles topical gel for treatment of pityriasis versicolor: formulation and clinical study. Drug Deliv., 2018; 25: 78-90.

42. Popat A, Liu J, Lu GQM, Qiao SZ. A pH-responsive drug delivery system based onchitosan coated mesoporous silica nanoparticles. J Mater Chem, 2012; 22: 11173-11178.

43. Khanal S, Adhikari U, Rijal NP, Bhattarai SR, Sankar J, Bhattarai N. pH-Responsive PLGA nanoparticle for controlled payload delivery of diclofenac sodium. J Funct Biomater. 2016; 7: 21.

44. Lo WH, Deng FS, Chang CJ, Lin CH. Synergistic antifungal activity of chitosan with fluconazole against Candida albicans, Candida tropicalis, and fluconazole-resistant strains. Molecules, 2020; 25: 5114.

45. Loquercio A, Castell-Perez E, Gomes C, Moreira RG. Preparation of chitosan-alginate nanoparticles for trans-cinnamaldehyde entrapment. J Food Sci., 2015; 80: 2305-2315.

46. Moazeni M, Saeedi M, Kelidari H, Nabili M, Davari A. An update on the application of nano-scaled carriers against fluconazole-resistant Candida species: nanostructured lipid carriers or solid lipid nanoparticles? Curr Med Mycol, 2019; 5: 8.

47. Walker L, Sood P, Lenardon MD, Milne G, Olson J, Jensen G, Wolf J, Casadevall A, Adler-Moore J, Gow NAR. The viscoelastic properties of the fungal cell wall allow traffic of AmBisome as intact liposome vesicles. mBio, 2018; 9: e02383-17.

48. Rodrigues ML, Travassos LR, Miranda KR, Franzen AJ, Rozental S, De Souza W, Alviano CS, Barreto-Bergte E. Human antibodies against a purified glucosylceramide from *Cryptococcus neoformans* inhibit cell budding and fungal growth. Infect Immun, 2000; 68: 7049–7060.

49. Silva LN, Ramos LDS, Oliveira SSC, Magalhães SC, Squizani LB, Kmetzsch ED, Vainstein LMH, Branquinha MH, Santos ALSD. Insights into the multi-azole resistance profile in *Candida haemulonii* species complex. J Fungi, 2020; 6: 215.

50. Zhang H, Niu Y, Tan J, Liu W, Sun MA, Yang E, Wang Q, Li R, Wang Y, Liu W, Global screening of genomic and transcriptomic factors associated with phenotype differences between multidrug-resistant and -susceptible *Candida haemulonii* strains. mSystems, 2019; 4: 1–17.

51. Maurya IK, Thota CK, Verma SD, Sharma J, Rawal MK, Ravikumar B, Sen S, Chauhan N, Lynn AM, Chauhan VS, Prasad R. Rationally designed transmembrane peptide mimics of the multidrug transporter protein cdr1 act as antagonists to selectively block drug efflux and chemosensitize azole-resistant clinical isolates of *Candida albicans*. J Biol Chem., 2013; 288: 16775-16787.

52. Haegler P, Joerin L, Krähenbühl S, Bouitbir J. Hepatocellular toxicity of imidazole and triazole antimycotic agents. Toxicol Sci., 2017; 157: 183-195.

53. Singh U, Dar MM, Anayutullah S, Alam H, Manzoor N, Al-Thabaiti SA, Hashmi AA. Design and synthesis of Co (II) and Cu (II) complexes of a dendrimeric chelate: promising anticandidal potential of chelotherapeutic agents. J Coord Chem., 2015; 68: 2096-2106.

54. Gupta M, Vyas SP. Development, characterization and in vivo assessment of effective lipidic nanoparticles for dermal delivery of fluconazole against cutaneous candidiasis. Chem Phys Lipids, 2012; 165: 454-461.

55. Herrada J, Gamal A, Long L, S. P. Sanchez, T. S. McCormick, M. A. Ghannoum, *In vitro* and *in vivo* antifungal activity of ambisome compared to conventional amphotericin b and fluconazole against *Candida auris*. Antimicrob. Agents Chemother, 2021; 65: e00306-21.

56. M. A. Khan, A. N. Aljarbou, A. Khan, H. Younus, Liposomal thymoquinone effectively combats fluconazole-resistant *Candida albicans* in a murine model. Int J Biol Macromol, 2015; 76: 203-208.

57. Nasr M, Teiama M, Ismail A, Ebada A, Saber A. In vitro and in vivo evaluation of cubosomal nanoparticles as an ocular delivery system for fluconazole in treatment of keratomycosis. Drug Deliv Transl Res, 2020; 10: 1841–1852.

58. Li XN, Zhang LM, Wang YY, Zhang Y, Jin ZH, Li J, Wang RR, Xiao WL. SWL-1 reverses fluconazole resistance in *Candida albicans* by regulating the glycolytic pathway. Front Microbiol, 2020; 11: 572608.

59. Wang T, Pan M, Xiao N, Wu J, Wang Q, Cheng T, Yan G, Wu D, Li N, Shao J. In vitro and in vivo analysis of monotherapy and dual therapy with ethyl caffeate and fluconazole on virulence factors of *Candida albicans* and systemic candidiasis. J Glob Antimicrob Resist, 2021; 27: 253-266.
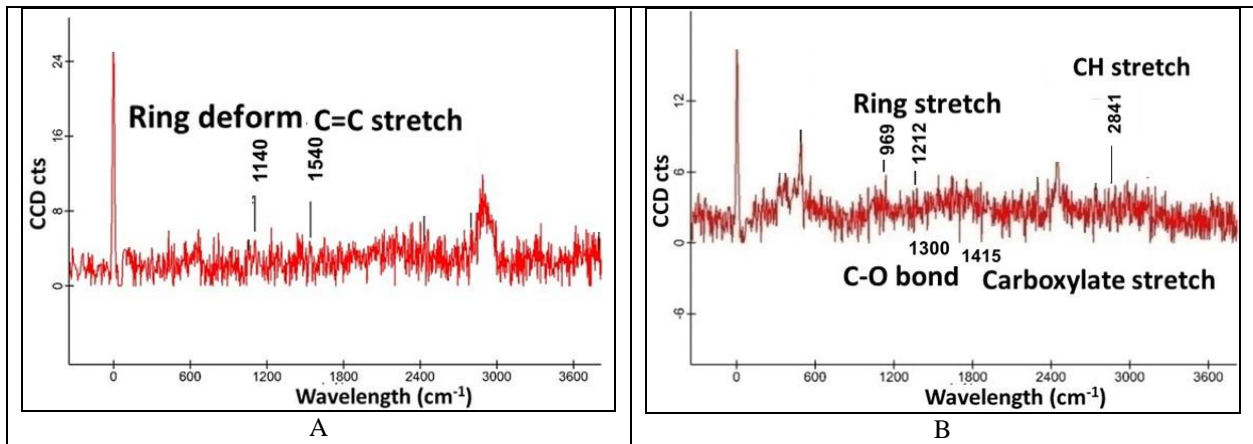
Supplementary Information

Figure S1: Characterization of nanoparticles. Raman spectroscopy of A) Fluconazole and B) C-Alg-NPs.
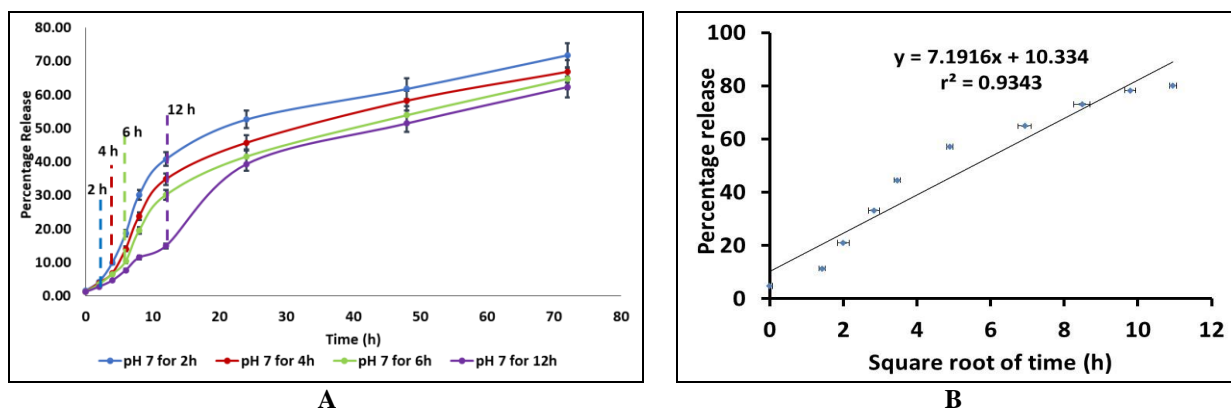

Figure S2: Drug release of fluconazole. A) pH shift assay: C-Alg-Fluc-NPs exposed to pH 7 at different time points (2, 4, 6, 12) and shifted to pH 4 upto 72 h. B) drug release at pH 4 followed the Higuchi model.
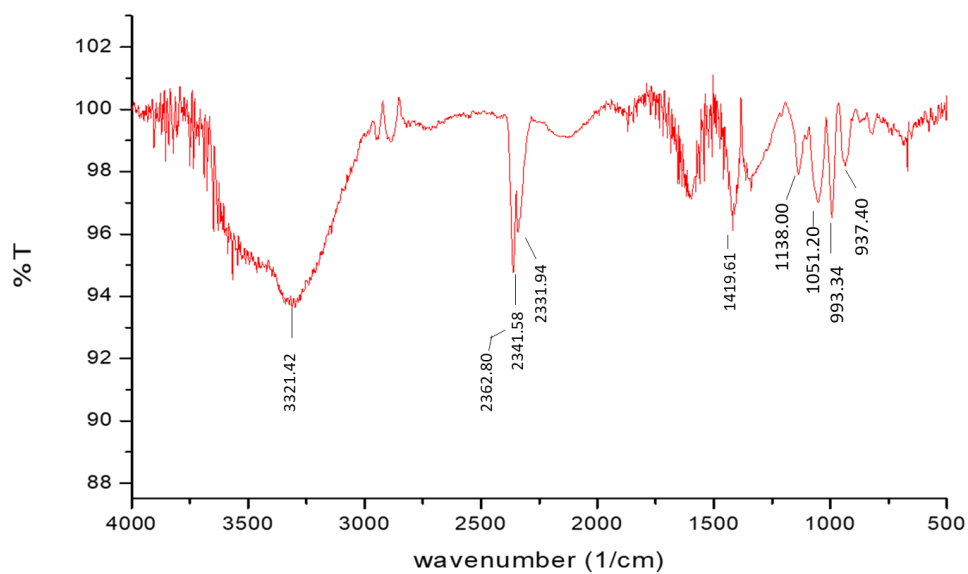

Figure S3: Characteristics of alginate. FTIR analysis of alginate.

Alginate. a linear copolymer of mannuronic (M) and guluronic acid (G) was used in the nanoformulation. The M/G ratio of alginate was tentatively estimated from specific absorption bands (808/787 cm^{-1} and 1030/1080 cm^{-1}) in infrared spectra (Supplementary Figure S3) according to Gómez-Ordóñez & Rupérez, 2011.

Mannuronic (M) and guluronic acid (G) are the main polysaccharide components found in sodium alginate. The M/G ratio of alginate was 1.08-1.15, suggesting higher values of mannuronic than guluronic acid blocks (M/G > 1).

Gómez-Ordóñez, E., & Rupérez, P. (2011). FTIR-ATR spectroscopy as a tool for polysaccharide identification in edible brown and red seaweeds. *Food hydrocolloids*, *25*(6), 1514-1520.

Table S1: MIC 90 values of C-Alg-Fluc and Fluc tested against fungal strains.

Sr No	Standard cultures	C-ALG-Fluc (µg/ml)	Fluc (µg/ml)
1	*Candida albicans NCIM 3100*	<1.25	80
2	*Candida auris NCCPF 470060*	2.5	160
3	*Candida glabrata ATCC 2001*	2.5	80
4	*Candida glabrata ILK7465*	<1.25	160
5	*Candida tropicalis ATCC 750*	1.25	80
6	*Candida krusei ATCC 6258*	<1.25	160
7	*Candida parapsilosis ILK2286*	<1.25	40
	Clinical isolates		
1	*Candida parapsilosis 1G*	1.25	80
2	*Candida tropicalis 1G*	<1.25	80
3	*Candida albicans1G*	<1.25	80
4	*Candida parapsilosis 2G*	1.25	40
5	*Candida glabrata1G*	<1.25	80

Table S2: Analysis of liver histological sections.

Group		Vascular changes- Congestion /Hemorrhages in hepatic parenchyma	Cellular changes, Swelling of hepatocytes, Degenerative and granular cytoplasmic changes, Vacuolar cytoplasmic changes	Loss of nuclei and necrotic changes of hepatocytes	Inflammatory changes in hepatic tissue, MNC infiltration in the hepatic parenchyma.	Overall Pathological grade / lesion score
i	Healthy Control	NAD	NAD	NAD	NAD	NAD
ii	Infected control	Focal (+1)	Focal (+1)	NAD	NAD	Minimal (+1)
iii	C-Alg-NPs	NAD	NAD	NAD	NAD	NAD
iv	Fluc 1	Focal (+1)	Focal (+2)	Focal (+1)	NAD	Mild (+2)
v	Fluc 2	Focal (+1)	Focal (+2)	Focal (+1)	NAD	Mild (+2)
vi	Fluc 3	Focal (+2)	Focal (+2)	Focal (+2)	Focal (+1)	Mild to Moderate (+3)
vii	C-Alg-Fluc 1	NAD	NAD	NAD	NAD	NAD
viii	C-Alg-Fluc 2	NAD	NAD	NAD	NAD	NAD
ix	C-Alg-Fluc 3	Focal (+1)	NAD	NAD	NAD	Minimal (+1)

Note: Overall Grade score as- NAD =No Abnormality Detected, Minimal changes (+1), Mild changes (+2), Moderate changes (+3), Severe changes (+4).